

IS M82 X-1 REALLY AN INTERMEDIATE-MASS BLACK HOLE? X-RAY SPECTRAL AND TIMING EVIDENCE

RALPH FIORITO¹ AND LEV TITARCHUK²

Received 2004 July 13; accepted 2004 September 9; published 2004 September 17

ABSTRACT

Ultraluminous X-ray sources (ULXs) with apparent luminosities up to hundreds of times the Eddington luminosity for a neutron star have been discovered in external galaxies. The existence of intermediate-mass black holes has been proposed to explain these sources. We present evidence for an intermediate-mass black hole in the ULX M82 X-1 based on the spectral features and timing (quasi-periodic oscillation [QPO]) properties of the X-radiation from this source. We revisited *XMM-Newton* and *Rossi X-Ray Timing Explorer (RXTE)* data for M82 X-1 obtained in 2001 and 1997 for *XMM* and *RXTE*, respectively. We show for these observations that the source is either in transition or in a high/soft state with photon spectral indices 2.1 and 2.7, respectively. We confirm the early determination of the QPO frequency $\nu \approx 55$ mHz in this source by Strohmayer & Mushotzky and identify this as the low-frequency QPO for the source. We apply a new method to determine the black hole mass of M82 X-1. The method uses the index-QPO low-frequency correlation that has been recently established in Galactic black hole candidates GRS 1915+105, XTE J1550–564, 4U 1630–47, and others. Using scaling arguments and the correlation derived from the consideration of Galactic black holes, we conclude that M82 X-1 is an intermediate black hole with a mass of the order of $1000 M_{\odot}$.

Subject headings: accretion, accretion disks — black hole physics — radiation mechanisms: nonthermal

1. INTRODUCTION

A number of external galaxies, notably ones with active star formation regions, have revealed the presence of so-called ultraluminous X-ray sources (ULXs), which one can operationally define as X-ray sources that are not coincident with the nucleus of their host galaxies and that have an apparent luminosity in excess of an order of magnitude above the Eddington luminosity for a neutron star ($L_x \gtrsim 10^{39}$ ergs s⁻¹). The high luminosity of ULXs have led to speculation that these objects may be intermediate-mass (10^2 – $10^4 M_{\odot}$) black holes (BHs; e.g., Colbert & Mushotzky 1999; Strohmayer & Mushotzky 2003, hereafter SM03; Shrader & Titarchuk 2003, hereafter ST03; Miller et al. 2003) or, more conservatively, beamed sources of lower mass (King et al. 2001). However, owing to their distances, the prospects for dynamical measurement of the mass of ULXs are poor and other means must be sought to identify their masses.

ST03 present the analysis of observational data for representative objects of several classes: Galactic black holes (GBHs), narrow-line Seyfert galaxies, and ULXs. They apply a methodology, which uses the spectral characteristics of the X-ray source radiation, to determine the mass. Using a color temperature from the bulk motion Comptonization (BMC) model, ST03 calculate the mass of several GBHs. Their results are in agreement with the masses obtained by optical or other methods when available. ST03 also calculate masses in ULXs for seven sources. The most compelling cases for the presence of intermediate-mass objects are NGC 1313 and NGC 5408, objects for which $\log(M/M_{\odot}) = 2.2$ and 3.0, respectively.

There are suggestions in the literature (see King et al. 2001) that the radiation from some ULXs is beamed and thus the real luminosity is much smaller than the Eddington luminosity for a solar mass BH (or neutron star). In fact, King et al. do not exclude

the possibility that *individual* ULXs may contain extremely massive BHs. But they emphasize that the formation of a large number of ultramassive BHs is problematic in terms of the evolutionary scenario of the binary systems. The recent discovery of the fast variability (quasi-periodic oscillation [QPO]) of the X-radiation in the ULX M82 by SM03 suggests that the X-ray emission area is quite compact in this particular source. In fact, for a jet of a typical size of about 10^{13} – 10^{14} cm, one cannot expect the QPO frequency $\nu \approx 50$ mHz that is observed by SM03 in M82 X-1. Thus, if the radiation from these variable sources is isotropic, then the high inferred luminosity of M82 X-1 requires an intermediate-mass BH, i.e., a BH more massive than one that can be formed in the collapse of a single normal star.

If ULXs are indeed accreting BHs with properties presumably similar to GBHs, similar observable properties, in particular, correlations of the X-ray spectral indices and QPO frequencies in ULXs, should be seen (see Vignarca et al. 2003; Titarchuk & Fiorito 2004, hereafter TF04; Titarchuk et al. 1998). TF04 show how the mass of one GBH source can be used to determine that of another, e.g., GRS 1915+105 and XTE J1550–564, which exhibit remarkably similar QPO frequency–index correlation curves (shown here as Fig. 1). Once the mass of one object (e.g., GRS 1915+105) is determined by a fit of theory to the measured QPO frequency–index correlation curve, the mass of the other (XTE J1550–564) can be found by simply scaling, i.e., sliding the correlation curve for GRS 1915+105 along the frequency axis until it coincides with the correlation curve of XTE J1550–564, in this case by the factor 12/10. Thus, the inferred mass of XTE J1550–564 is 10/12 times less than that of GRS 1915+105. The mass determination using the QPO frequency–index correlation fit is consistent with X-ray spectroscopic and dynamical mass determinations for these sources (see references in ST03). Since QPO frequencies are inversely proportional to the mass of the central object, one can, in principle, determine the mass of a ULX using the same kind of scaling as described above for GBHs. It is important to note the BH mass determination method using the QPO-index correlation is independent of the orientation of the source. In fact, the photon

¹ University of Maryland, College Park; and NASA Goddard Space Flight Center, Greenbelt, MD 20771; rfiorito@milkyway.gsfc.nasa.gov, rfiorito@umd.edu.

² George Mason University/CEOSR, Fairfax, VA 22030; and US Naval Research Laboratory, Code 7655, Washington, DC 20375; ltitarchuk@ssd5.nrl.navy.mil and lev@lheapop.gsfc.nasa.gov.

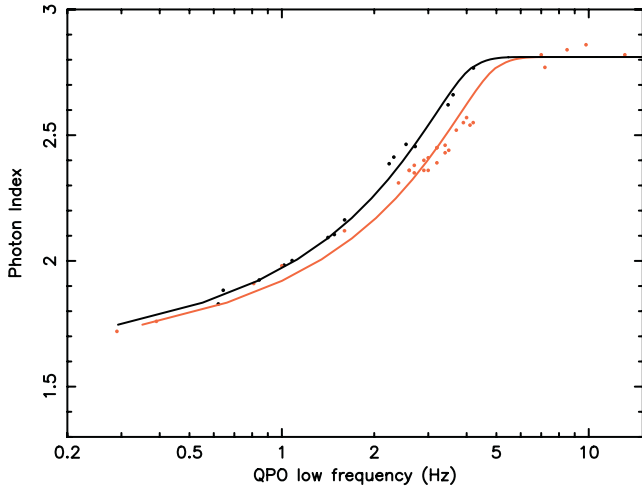


FIG. 1.—Comparison of the observed (filled circles) and the theoretical (solid lines) correlations of photon index vs. QPO low frequency between GRS 1915+105 (observations by Vignarca et al. 2003) and XTE J1550–564 (observations by Sobczak et al. 1999, 2000; Remillard et al. 2002a, 2002b; see also Figs. 6 and 8 in Vignarca et al. 2003). The black circles and line are for GRS 1915+105, and the red circles and line are for XTE J1550–564. The XTE J1550–564 curve is produced by sliding the GRS 1915+105 curve along the frequency axis with a factor 12/10 (see text for details).

index of the Comptonization spectrum is a function of the Comptonization parameter only, which is a product of the mean energy change at any photon scattering and the mean number of scatterings in the Compton cloud (corona; see, e.g., Sunyaev & Titarchuk 1980).

In § 2, we present the results of our spectral and timing analysis of archival *XMM* and *Rossini X-Ray Timing Explorer* (*RXTE*) data from the ULX M82 X-1. In § 3, we discuss our results of the data, compare them to those presented by SM03, and employ our results to estimate the mass of M82 X-1. Conclusions also follow in § 3.

2. DATA ANALYSIS AND RESULTS

We have revisited archival spectral and timing *XMM* and *RXTE* data from the ULX M82 X-1, which has been previously investigated by SM03 and Rephaeli & Gruber (2002, hereafter RG02). We analyzed four archival observations: (1) the *XMM* European Photon Imaging Camera (EPIC) PN and MOS data from the 30 ks observation 2001 May 5 (observation ID [ObsID] 0112290201) and (2) the *RXTE* Proportional Counter Array (PCA) data from 1997 archival observations of RG02 (ObsIDs 20303-02-02 [2.5 ks], 20303-02-03 [4.76 ks], and 20303-02-04 [2.5 ks]). The latter two observations show the presence of QPOs and a power-law (PL) component in their energy spectra, which we have reanalyzed in terms of the transition layer model previously applied by us to the study of GBH sources (TF04). We were not able to identify the QPO reported by SM03 for ObsID 20303-02-02 (2.5 ks).

2.1. Energy Spectra

XMM data.—We extracted the spectrum of M82 X-1 from both the EPIC MOS and PN images of M81 in a circle of 18" in radius around the bright source (M82 X-1), using the latest version of the SAS data reduction software and response matrices. We focused our attention on the energy range 3.3–10 keV, where interference from the soft diffuse component surrounding the bright source is minimized. We find that this energy range

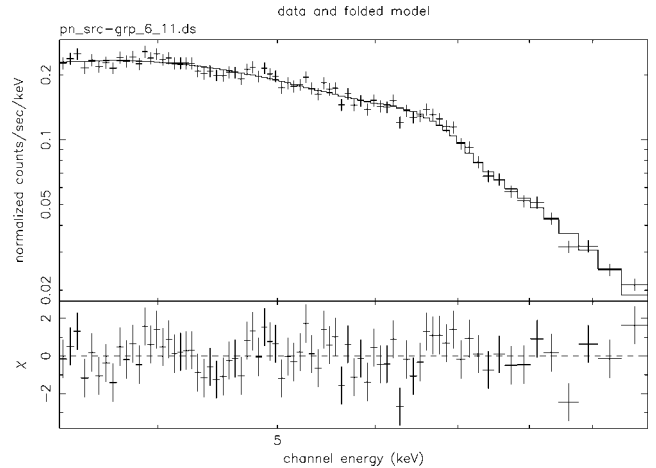


FIG. 2.—BMC fit to the *XMM* PN energy spectrum of M82 X-1 in the range 3.3–10 keV.

gives more consistent results for the spectral modeling and timing analysis than that used by SM03 (2–10 keV); i.e., increasing the lower energy value from 2 to 3.3 keV produced the lowest value of residuals in our energy spectral fits ($\chi^2_{\text{red}} \leq 2$) and had virtually no effect on the χ^2_{red} and parameter values of our fits to the power spectrum when compared to those using the energy range 2–10 keV. Using XSPEC (ver. 11.3), we find that an absorbed PL model with a Gaussian iron line component and the BMC model (Titarchuk et al. 1997) with a Gaussian iron line component fixed at 6.5 keV and a line width of 0.4 keV give equally good fits ($\chi^2_{\text{red}} \leq 1$), when the column density is left as a free parameter. Since the real column density is unknown, because of the obscuration effect of the surrounding diffuse emission surrounding M82 X-1, we allow this parameter to be free. The χ^2_{red} and fitted parameters showed little change with temperature up until $kT = 0.5$ keV. In order to obtain the index, normalization, and column density, we fixed the value of kT below this value, i.e., $kT = 0.1$ keV. We find that for the best-fit spectrum the contribution of the Comptonized component in the BMC spectrum is dominant. The BMC model spectrum is a sum of the (disk) blackbody component and Comptonized blackbody component, where $A/(1 + A)$ is a relative weight of the Comptonized component. Because all values of parameter $A \gg 1$ are consistent with observations, we fixed $\log A$ to 5. With these constraints, we find that the PL index and column densities from the PL and BMC fits give close to the same results for all the observations investigated by us. We also noticed that an absorbed multitemperature thermal disk model (diskBB) with a Gaussian provides a statistically good fit but that a high disk temperature ($T_i \sim 3$ keV) is required, in agreement with the results of SM03. An example of a fit to our reduced PN data using the BMC-Gaussian Fe line model is given in Figure 2. A comparison of fits to our reduced data for the PL and BMC models with that produced by SM03 for the energy band 3.3–10 keV yields nearly identical results. Fits to the MOS data (similar data are mentioned but not presented in SM03) give close to the same fitted parameters as the PN data fits.

RXTE data.—Spectra from M82 were also obtained from the archival observations of RG02 (using PCA standard products and the epoch 3 response matrix). A comparison of the free spectral fit parameters for the *XMM* EPIC PN and MOS and *RXTE* PCA data is given in Table 1. Based on the photon indices obtained from the *XMM* PN observation, we conclude that the source was in a transition from hard to soft state, i.e., characterized by an index between 1.5 and 2.5, for the time

TABLE 1
THE BEST-FIT SPECTRAL PARAMETERS

ObsID	Instrument	$n_{\text{H(PL)}} \times 10^{22}$	$n_{\text{H(BMC)}} \times 10^{22}$	Γ_{PL}	Γ_{BMC}	$N_{\text{BMC}} \times 10^{-3}$
011201	<i>XMM</i> PN	7.50 ± 0.69	7.50 ± 0.69	2.07 ± 0.07	2.07 ± 0.07	0.26 ± 0.08
011201	<i>XMM</i> MOS	6.98 ± 1.17	7.42 ± 1.21	1.71 ± 0.14	1.82 ± 0.16	0.21 ± 0.13
20303-02-02	<i>XTE</i> PCA	3.73 ± 0.76	4.43 ± 1.53	2.62 ± 0.09	2.65 ± 0.13	1.13 ± 0.67
20303-02-03	<i>XTE</i> PCA	4.09 ± 0.78	5.26 ± 1.93	2.46 ± 0.09	2.52 ± 0.13	1.11 ± 0.67
20303-02-04	<i>XTE</i> PCA	6.06 ± 0.81	5.21 ± 0.85	2.67 ± 0.09	2.63 ± 0.1	1.35 ± 0.55

period of the *XMM* observation, and that for the period of the *RXTE* data reported here the source was in a soft state (i.e., spectral index ~ 2.5).

2.2. Timing Analysis

XMM data.—We extracted a light curve from the EPIC PN instrument selected, from the same image area described in § 2.1 in the energy band 3.3–10 keV with a 1 s time bin and one 30 ks window, which includes all the PN data. From this light curve, we computed the power spectra using the current release of the XRONOS program. The power spectrum was rebinned a factor of 256 to obtain the results shown in Figure 3 (left), which exhibits a clear QPO. The high error in the red noise portion of the power spectra below 30 mHz does not allow a determination of the expected break frequency below the QPO frequency. Thus, we cannot reliably identify the break frequency, which is usually found with the QPO low frequency in GBH sources, from the *XMM* data (see Wijnands & van der Klis 1999). The data suggest but do not confirm the presence of a peak at approximately 100 mHz, but the statistics are too poor to positively identify this frequency (see also the *XMM* data of SM03). Because of the severity of the red noise below 30 mHz, we have, following SM03, chosen to fit the power spectrum with a model consisting of a constant to account for the Poisson noise, a simple PL to account for the red noise, and a Lorentzian to account for the presence of the QPO. Our fit to the data using this model gives a good fit of $\chi^2 = 47$ for 58 degrees of freedom, $\nu_{\text{QPO}} = 58.5 \pm 1.7$ mHz, $\Delta\nu_{\text{QPO}}/2 = 5.8 \pm 1.5$ mHz, and $A_{\text{QPO}} = 0.011 \pm 0.003$, which are in good agreement with the more accurate results obtained by SM03 using all three EPIC instruments. Here A_{QPO} represents the total rms power in the QPO, and $\Delta\nu_{\text{QPO}}$ is the FWHM of the QPO. We checked the significance of the QPO by observing that $\chi^2 = 70$ when the QPO was excluded from the model. Using

the *F*-test, one finds the probability $\approx 3 \times 10^{-5}$ for a random occurrence of the QPO feature. These results give us great confidence that the QPO is observed by the PN instrument (cf. SM03).

RXTE data.—We extracted a light curve using good time intervals and 3–10 keV energy selected power density spectra (PDSs) from the three *RXTE* ObsIDs listed above, employing a 128 Hz sampling rate and only the top xenon layers of the operating Proportional Counter Units for each observation time interval. The IDL program RADPS, written by C. Markwardt, was used to produce the PDS averaged over several 1024 s intervals for each light curve. We clearly identified single QPOs in the PDS for two of the three ObsIDs studied by SM03. We fit our PDS data to a sum of two Lorentzian peaks, and the lowest or zero-order Lorentzian was picked to identify the red noise break frequency of the PDS. A clearly identifiable break frequency at 26 ± 2.5 mHz with $A_{\text{br}} = 4.8 \pm 0.4$ confirmed by a plot of frequency time power versus frequency, coincident with a QPO at 106 ± 2 mHz and $A_{\text{QPO}} = 0.095 \pm 0.018$, was observed for ObsID 20303-02-04. A QPO at 48.9 ± 1 mHz and $A_{\text{QPO}} = 0.04 \pm 0.013$ was also observed for ObsID 20303-02-03, but a clearly definable break frequency was not observed for this ObsID. Lorentzian line fits to the PDS for the former case are presented in Figure 3 (right). We also looked for variation of the total variability as a function of energy by observing the variability in two energy bands, 3–6 keV and 6–10 keV, but no variation was observed.

3. DISCUSSION AND CONCLUSIONS

The spectral data for M82 X-1 definitely show the spectral features of the high/soft spectral phase when the photon indices Γ are in the range of 2–2.7. For the *XMM* PN ObsID and the *RXTE* 20303-02-04 ObsID, we find $\Gamma = 2.07 \pm 0.07$ and $\Gamma = 2.67 \pm 0.1$, respectively; the former value is characteristic

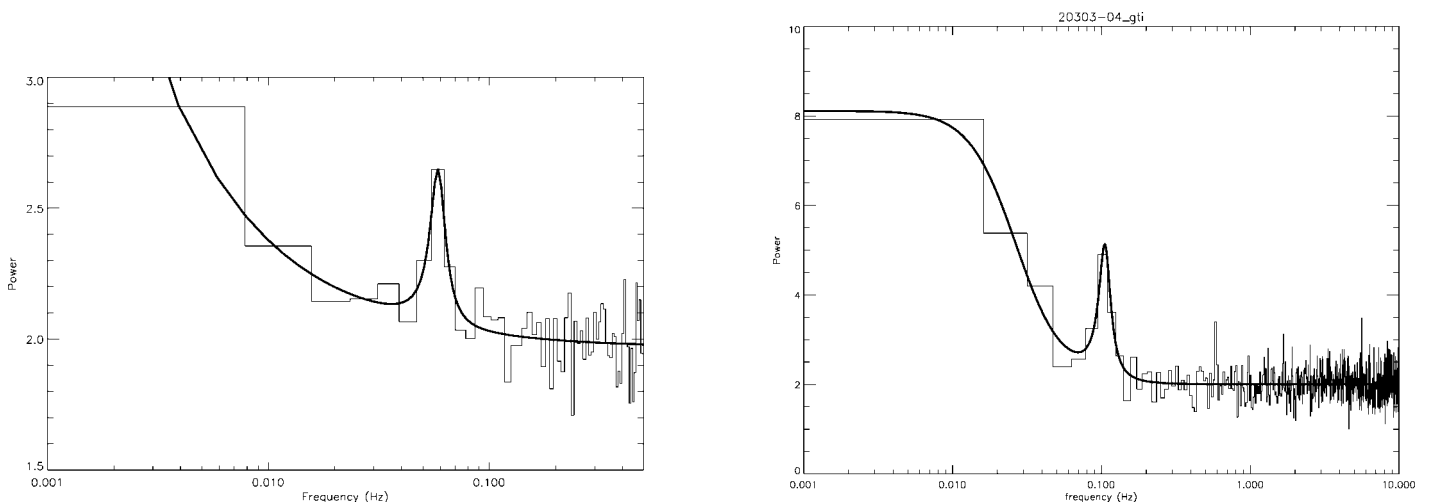


Fig. 3.—Left: Power spectrum from the *XMM* EPIC PN instrument for the source M82 X-1 for the energy range 3.3–10 keV, showing a QPO at 57 mHz. Right: Power spectrum for *RXTE* ObsID 20303-02-04, showing a break frequency at 26 mHz and QPO frequency at 106 mHz.

of a transition to the high/soft state, and the latter to the high/soft state. In these observations, two QPO frequencies, ~ 50 and ~ 100 mHz, have been identified. We interpret and identify the observed $\nu_{\text{QPO}} \sim 50$ mHz as the fundamental low frequency and $\nu_{2, \text{QPO}} \sim 100$ mHz as its first harmonic. We note that the presence of one predominant QPO, i.e., 50 or 100 mHz in different observations, is not an unusual occurrence (see, e.g., TF04) and can be explained as the result of the local driving frequency conditions in the coronal region; i.e., a resonance condition is established for one particular eigenmode of the compact coronal region so that this mode is predominantly observed. In other cases, for example, in GRS 1915+105 (Fiorito et al. 2003), the fundamental and first harmonics of the low-frequency QPO (along with break frequencies) are simultaneously observed. Such features are seen in a variety of other GBH sources as well. Also the proximity of the inferred fundamental $\nu_{\text{QPO}} \sim 50$ mHz to the observed break frequency, $\nu_b \sim 26$ mHz is similar to what is observed in GBHs.

If we identify $\nu_{\text{QPO}} \sim 50$ mHz as the low-frequency QPO frequency ν_{low} keeping in mind that $\Gamma \sim 2.7$ and $\nu_{\text{low}} \sim 5$ Hz for $10 M_{\odot}$ (see Fig. 1 for the index–QPO frequency correlation in XTE 1550–564) and the fact that ν_{low} is inversely proportional to M , we calculate $M \sim 5(\text{Hz})/0.050(\text{Hz}) \times 10 = 10^3 M_{\odot}$. As we show above (see also TF04), this scaling has been observed for GBHs, but this is the first time it has been applied to a ULX (M82 X-1) to estimate the BH mass. This value of BH mass is consistent with mass evaluations obtained using the absolute normalization and color temperature of other ULXs (NGC 253, NGC 1399 X-2, X-4, and IC 342 X-1), which have been analyzed

by ST03. We note the possibility that the 50 mHz QPO may not be the lowest intrinsic QPO frequency and that a lower one, which may be obscured by the red noise at frequencies $\nu_{\text{QPO}} < 50$, may exist. Therefore, the frequency $\nu_{\text{QPO}} \sim 50$ should be interpreted as an upper limit and the inferred BH mass as a lower limit. To conclude, we have presented a reanalysis and new interpretation of *XMM-Newton* and *RXTE* data obtained from M82 X-1. This analysis presents the BMC model spectral photon indices 2.1–2.7, which are seen in the high/soft states of extragalactic BHs and GBHs, and the identification of $\nu_{\text{QPO}} \sim 50$ mHz as an observable upper limit on the low-frequency QPO for M82 X-1. Using this value for the low QPO frequency, the predominantly observed spectral index ~ 2.7 , and the index–QPO frequency correlation recently obtained for GBHs establishes a lower limit of the mass of M82 X-1 of the order of $1000 M_{\odot}$. The demonstrated application of our method, which uses the low QPO frequency and the index of the PL component of the spectra, presents a new, potentially powerful tool for determining the nature and mass of ULXs. However, the confirmation of a ULX as an intermediate BH awaits the simultaneous application of the two independent methods we have described above, i.e., the ST03 method and QPO low-frequency–index correlation or direct dynamical evidence.

R. F. gratefully acknowledges helpful discussions with T. Strohmayer, C. Markwardt, and L. Angelini. L. T. acknowledges the support of this work by the Center for Earth Observing and Space Research of George Mason University.

REFERENCES

- Colbert, E. J. M., & Mushotzky, R. F. 1999, *ApJ*, 519, 89
 Fiorito, R., Markwardt, C., & Swank, J. 2003, AAS HEAD Meeting, 35, 11.07
 King, A. R., et al. 2001, *ApJ*, 552, L109
 Miller, J., et al. 2003, *ApJ*, 585, L37
 Remillard, R., et al. 2002a, *ApJ*, 564, 962
 ———. 2002b, *ApJ*, 580, 1030
 Rephaeli, Y., & Gruber, D. 2002, *A&A*, 389, 752 (RG02)
 Shrader, C., & Titarchuk, L. G. 2003, *ApJ*, 598, 168 (ST03)
 Sobczak, G. J., et al. 1999, *ApJ*, 517, L121
 Sobczak, G. J., et al. 2000, *ApJ*, 531, 537
 Strohmayer, T. E., & Mushotzky, R. F. 2003, *ApJ*, 586, L61 (SM03)
 Sunyaev, R. A., & Titarchuk, L. G. 1980, *A&A*, 86, 121
 Titarchuk, L. G., & Fiorito, R. 2004, *ApJ*, 612, 988 (TF04)
 Titarchuk, L. G., Lapidus, I. I., & Muslimov, A. 1998, *ApJ*, 499, 315 (TLM98)
 Titarchuk, L. G., Mastichiadis, A., & Kylafis, N. D. 1997, *ApJ*, 487, 834
 Vignarca, F., et al. 2003, *A&A*, 397, 729 (V03)
 Wijnands, A. D., & van der Klis, M. 1999, *ApJ*, 514, 939